A Temperature-Dithering Closed-Loop Interface Circuit for a Scanning Thermal Microscopy System

Joohyung Lee and Yogesh B. Gianchandani, *Senior Member, IEEE*

***Abstract*—This paper presents an interface circuit for low-frequency dithering measurements of resistor-based transducers. It is demonstrated in the context of a polyimide-shank scanning thermal microscopy probe which provides high thermal sensitivity and spatial resolution, but has a low bandwidth from both mechanical and thermal perspectives. These pose challenges in temperature dithering and control, as well as noise immunity. The circuit includes a proportional-integral controller and a demodulator, along with appropriate amplifier and filter blocks. It keeps the average temperature of the probe tip constant while synchronously detecting variations in the second harmonic of the modulated signal as the tip is scanned across the sample surface. Strategic choices in the circuit architecture and topology are evaluated, and the overall system including the sensor and the circuit is simulated. Measurements of the implemented system show that a signal-to-noise ratio (SNR) of 15.7 is achieved while scanning a photoresist sample of 218 nm thickness on a silicon substrate, and that the detection limit for variations in thermal conductance is $< 3\ \mathrm{pW/K}$. [1125]**

***Index Terms*—Polyimide probe, scanning probe, thermal imaging.**

I. Introduction

SCANNING thermal microscopy was introduced in 1986 by Williams and Wickramasinghe and was followed by the development of various thermal probes such as the thermocouple (TC) [18], [27], [7], [20], [31], the bolometer or wire resistor [3], [9], Schottky diode [2], [12], and bimaterial cantilever [1], [22]. Applications of this technology include deep submicron lithography research, cellular diagnostics in biochemistry [23], [15], data storage, and other applications [30], [29], [19], [8]. The lithographically micromachined probes are generally made from dielectric thin films on a silicon substrate, and use additional metal or semiconductor layers for sensing purposes. Other approaches that use more involved micromachining methods have also been reported [7].

In a bolometer probe, the resistor can be used as a local heater while the fractional change in probe resistance is used to detect temperature and/or thermal conductance of the sample, which makes it amenable for applications such as thermal conductance mapping and microcalorimetry. Thermal conductance mapping, which is of particular interest in this effort, is performed by monitoring the variation of the thermal load on a heated probe as it is rastered across the sample. (In the case of a thin film sample, for example, if it is assumed that the underlying substrate wafer or the sample chuck is at constant temperature, the thermal load on the probe tip is related to variations in the thermal conductance of the sample.) A commercially available Wollaston wire probe [28] uses a narrow gauge wire bent into a V-shape to form a self-supporting resistor. The wire has a thin platinum/rhodium (90/10) core of 5 $\mu\mathrm{m}$ diameter, surrounded by a thick silver cladding of 75 $\mu\mathrm{m}$ diameter. It has been used for various thermal analyses [4]–[6], [9]. However, probes with smaller scanning tips are needed for high spatial resolution. In addition, for many applications, the probes must have very low mechanical spring constants to prevent damage to soft samples, while for certain applications in which small amounts of heat generated from the sample have to be detected, they must have very high thermal isolation to minimize the thermal load presented to it. All of these needs can be met by a lithographically micromachined probe having a compliant polyimide shank with high thermal resistance [15]. However, thermal and mechanical challenges such as these must be evaluated in conjunction with the interface circuit for the best performance of the overall system.

In techniques such as atomic force microscopy, the measurement of small variations across a sample surface is commonly facilitated by modulation of the detected signal. This is akin to chopping an optical signal, and permits the detection to be phase-locked to the dither, improving the overall signal-to-noise ratio (SNR). While it is possible to dither the supplied heat by photothermal means [24], [17], [26], e.g., with a laser diode, an approach that is more widely used is to mechanically dither the heated tip so that the tip-to-sample spacing is modulated. The precise mechanical dithering motion is usually realized by an electrostatic or piezoelectric actuator, while the tip is operated in a noncontact mode. However, the temperature sensitivity of the probe is compromised because of the large thermal resistance of the air gap. Furthermore, the effective sensing area is enlarged as the distance between the sensor and the sample increases, compromising spatial resolution. In addition, this approach requires high stiffness in the probe, and is inappropriate for the type of ultracompliant probe with low spring constant that is used in this effort.

Another option for dithering the heat supplied to the probe is to modulate the current in the embedded bolometer. In one approach known as the 3ω technique [21], [16], [4], an ac electric current of the form $I_o \sin(\omega_o t)$ is fed into the resistive el-

Manuscript received July 31, 2003; revised May 20, 2004. This work was supported in part by the Semiconductor Research Corporation under Contract 98-LP-452.005. The Center for NanoTechnology, University of Wisconsin-Madison, is supported in part by a DARPA/ONR Grant MDA 972-00-1-0018 and MDA 972-99-1-0013. Subject Editor T. Kenny.

J. Lee was with the Electrical and Computer Engineering Department, University of Wisconsin, Madison, WI 53706 USA. He is now with Samsung Electronics, Gyeonggi-Do, Korea (e-mail: jhyung.lee@samsung.com).

Y. B. Gianchandani was with the Electrical and Computer Engineering Department, University of Wisconsin, Madison, WI 53706 USA. He is now with the Electrical Engineering and Computer Science Department, University of Michigan, Ann Arbor, MI 48109 USA (e-mail: Yogesh@umich.edu).

Digital Object Identifier 10.1109/JMEMS.2004.839011

1057-7157/$20.00 © 2005 IEEE

ement. It creates a temperature fluctuation at frequency $2\omega_o$, and consequently a resistance fluctuation at $2\omega_o$ as well. This further leads to a voltage fluctuation at $3\omega_o$ across the resistive element. Making use of the frequency dependence of the resulting temperature oscillations enables the determination of the thermal conductivity. However, the average tip temperature depends upon the ac temperature variation, and necessitates an additional means of heating or cooling to maintain a constant temperature during a scan.

This paper [1] presents an interface circuit intended to be used with a probe that is mechanically ultracompliant and cannot be physically dithered. It uses a proportional-integral (PI) controller to set the bias current through the bolometer, and thus the tip temperature, to a user-defined value. The dithered heating is achieved by superimposing a relatively small sinusoidal signal on a dc bias voltage across the sensing bolometer. The resulting output signal has components at both ω_o and $2\omega_o$. (The $3\omega_o$ component also exists, but is negligible.) The $2\omega_o$ component is selected for the output in order to minimize the impact of $1/\mathrm{f}$ noise from the interface circuit, which includes temperature controller and demodulator. Compared to the 3ω method, the proposed method is more easily scaled for multiprobe systems. The sample temperature is electrically controlled by dc power without additional heating tools, while ac power is used to dither the thermal signal. The sensed signal is detected through a resistor bridge, and then demodulated by the circuit, which contains the necessary amplification and filtration stages as well. The principle, approach, and compromises related to the design choices are described in Section II. The circuit is modeled together with the electrothermal characteristics of the probe in Section III. Measured performance of the selected implementation of the circuit obtained during the practical scan of a sample are examined in Section IV.

II. System Description

A. Sensor Element

Fabrication: The scanning thermal probe is fabricated on a Si substrate using a 7-mask process as reported in [13], [14], and [10]. It is briefly described here for completeness. A metal thin film bolometer is sandwiched between two layers of polyimide that form a cantilever. At one end of the cantilever the Ni thin film protrudes through an opening in lower polyimide layer, where it is molded into a pyramidal tip by a notch that is anisotropically wet-etched into the substrate. The tip and a portion of the probe shank are then released from the substrate by etching an underlying sacrificial layer. The released length is then folded over to extend past the die edge for clearance, and held in place by a thermocompression bond across a thin film of Au which is deposited as the final layer on top of the polyimide, as shown in Fig. 1. Typical dimensions of the probes after assembly are 360 $\mu\mathrm{m}$ length, 120 $\mu\mathrm{m}$ width, and 3.5 $\mu\mathrm{m}$ thickness with Cr/Ni (20/100 nm) for the tip and Cr/Au (20/200 nm) for the lead, resulting in a bolometer resistance of 45 Ω. The probes offer lateral spatial resolution of < 50 nm, and mechanical spring constants ranging from 0.1 to 0.3 N/m depending on the dimension of the probes. In comparison, Wollaston wire probes typically provide spatial resolution > 1 $\mu\mathrm{m}$, spring constant > 1 N/m, and can be subject to substantial variations resulting from a nonlithographic manufacturing process.

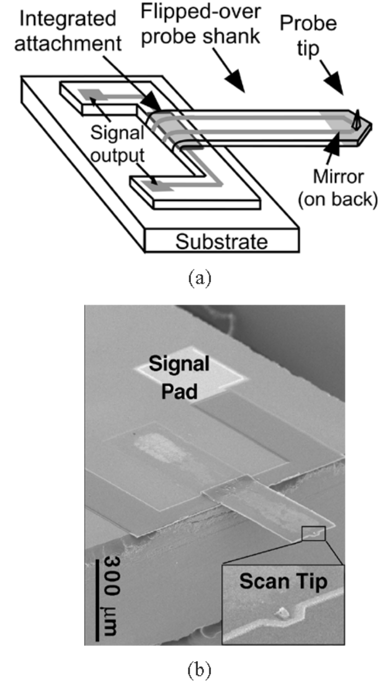

Fig. 1. Ultracompliant scanning thermal probe. (a) Schematic of a polyimide thermal probe. (b) SEM image of a fabricated thermal probe with a close up of the scan tip.

Operation: For limited temperature excursions in metal and semiconductor materials, the electrical resistance can be approximated as being linearly proportional to the average probe temperature:

$$R_p = R_o \cdot [1 + TCR \cdot (T - T_o)] \quad (1)$$

where R_o is the resistance at room temperature T_o and *TCR* is the temperature coefficient of resistance. If the parasitic resistance can be ignored, the resistance change is linearly proportional to the square of the applied current. Therefore, (1) can be rewritten as

$$R_p = R_o \cdot [1 + TCR \cdot \beta \cdot I_p^2] \quad (2)$$

where β is a unit-converting constant in $\mathrm{K/A^2}$, and I_p is the current through the probe. According to (2), the probe resistance is linearly proportional to the applied power. This has been experimentally verified. A typical value for the $TCR \bullet \beta$ factor is 520.8 when the current I_p is less than 0.01 A.

B. Interface Circuit

The readout approach used in this effort is illustrated in Fig. 2. As the probe scans the sample surface, a topographic image is produced by detecting the laser beam reflected from the surface of the probe while the mechanical feedback loop maintains a constant contact force. As indicated previously, the circuit uses

[1]Portions of this paper have been presented in conference abstract form in [11].

Fig. 2. A scanning thermal microscopy sensing system equipped with a servo-controlled interface circuit using electrical temperature dithering and an ultracompliant micromachined thermal sensor.

a Wheatstone bridge interface to the probe, and includes a PI controller, a demodulator, and appropriate amplifier and filter blocks. The error voltage between bridge nodes is amplified by an instrumentation amplifier and then fed into the PI controller, which provides compensation current I_p to keep the bridge balanced. Since the average probe temperature increases or decreases with the compensation power, the probe resistance R_p is adjusted by I_p until the bridge regains balance. The PI controller is realized by using an integrator, an inverting amplifier, a summing amplifier, and a current buffer. High integral gain K_i of 1–2 $\times 10^4$ is chosen to achieve a fast response time.

For demodulation of the dithered signal, two of the options considered are shown in Fig. 3. The quadrature homodyne technique with downconversion, shown in Fig. 3(a), has been widely used in communication circuits, and offers high efficiency of power transfer. However, quadrature mixing requires shifting either the input or the local dither oscillator output by 90°. Either way, the errors in the nominally 90°-phase shifts and the mismatches between the amplitudes of the two references corrupt the signal. While it is possible to circumvent these challenges by adding more elements to the circuit, this is undesirable, particularly if multiple copies are needed for high-throughput multiprobe scanning.

Fig. 3(b) illustrates a simple homodyne demodulation technique. Not only does it require fewer components than the other options described (and is thereby a candidate for multiprobe systems), but also alleviates many of the problems with mismatches. However, it is not without compromise. Ideally, the phase of the local oscillator should be synchronized to that of the input carrier, i.e., the phase difference between input carrier signal and local oscillator must be small to prevent the distortion and attenuation of the output signal. In the context of the thermal probe, the implication is that the time-varying thermal delay associated with probe structure is negligible or is separately compensated.

When both a dc and an ac signal (at ω_o) are applied to the bridge through an emitter follower, as shown in Fig. 2, the bolometer is modulated by the square of $V_{\rm bridge} = V_{\rm dc} + V_{\rm ac} \cdot \cos(\omega_o t + \theta)$. The resulting change in the bolometer resistance is proportional to

$$\Delta R_p \propto I_{\rm dc}^2 + 2 \cdot I_{\rm dc} \cdot I_{\rm ac} \cdot \cos(\omega_o t + \theta) + I_{\rm ac}^2 \cdot \cos^2(\omega_o t + \theta) \quad (3)$$

and can be approximated by

$$R_p \cong R_{pDC0} + R_{pAC0} \cdot \cos(\omega_o t + \theta) \quad (4)$$

when $V_{\rm ac}^2 \ll 2 \cdot V_{\rm dc} \cdot V_{\rm ac}$.

The modulated ac resistance contains information on the thermal conductance of the sample. Supposing that the bridge circuit is balanced, such that its differential output is zero in the absence of a sample. Then, in the presence of a sample, the output of the bridge voltage difference amplifier primarily contains

$$V_2 - V_1 \cong \frac{1}{2} \cdot I_{\rm ac} \cdot R_{pAC} \cdot \cos(2\omega_o t + \theta) + I_{\rm dc} \cdot R_{pAC} \cdot \cos(\omega_o t + \theta) \quad (5)$$

where R_{pAC} represents the change in the ω_0 component of the probe resistance in the presence of the sample. Then, the output of integrator can be represented as

$$V_{\rm integ} \propto \frac{1}{\omega_o \cdot C \cdot R} \times \left\{ \frac{1}{4} \cdot I_{\rm ac} \cdot R_{pAC} \cdot \sin(2\omega_o t + \theta) + I_{\rm dc} \cdot R_{pAC} \cdot \sin(\omega_o t + \theta) \right\} \quad (6)$$

where C and R are the capacitor and resistor of the integrator, respectively. If the $2\omega_o$ term of (6) is selected, much of the thermal noise of the bridge can be eliminated. Better SNR is expected as $I_{\rm ac}$ becomes dominant. Even though the integrator output is fed back into the bridge circuit, its sinusoidal impact can be ignored as its ac amplitude is only a few percent of the modulating ac input of the bridge circuit.

In implementing the demodulation circuit, second-order biquad band-pass filters and low-pass filters are used as shown in Fig. 4 [25]. The transfer function of a biquad band-pass filter can be represented as

$$\frac{V_o}{V_i} = \frac{A \cdot \frac{\omega_1}{Q} \cdot s}{s^2 + \frac{\omega_1}{Q} s + \omega_1^2} \quad (7)$$

where $A = R_2/R_1$, $\omega_1 = 1/R_3 C$, and $Q = R_2/R_4$ Its gain, A, and center frequency, ω_1, can be separately controlled by changing R_1 and R_3, respectively, allowing both gain and phase mismatch to be minimized. The biquad band-pass filter has favorable tuning features, removing ω_o and dc components which are mixed in its input. The quality factor, Q, is determined by R_2 and R_4, and can reach 100 or more, beyond the capability of the other options. Fig. 4(b) shows the biquad low-pass filter

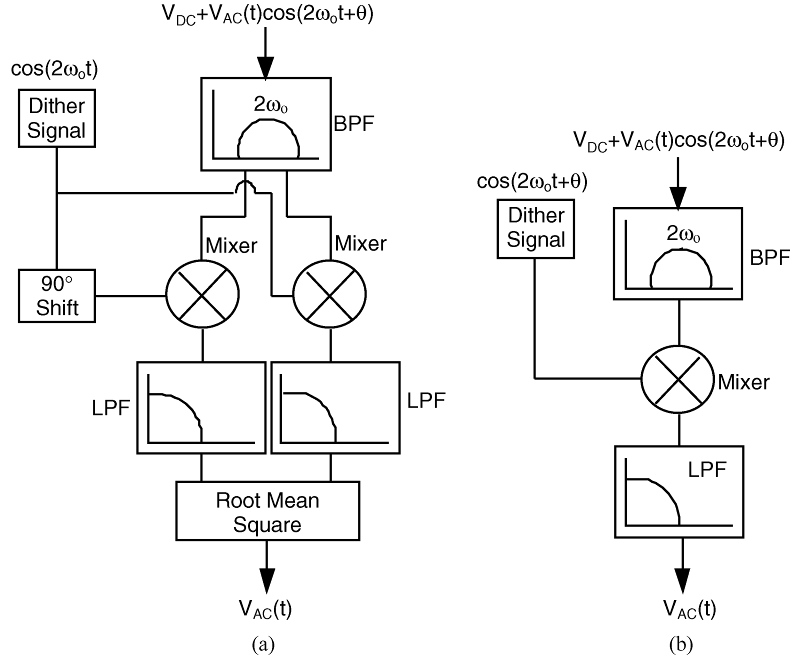

Fig. 3. Demodulation techniques. (a) Quadrature homodyne. (b) Simple homodyne.

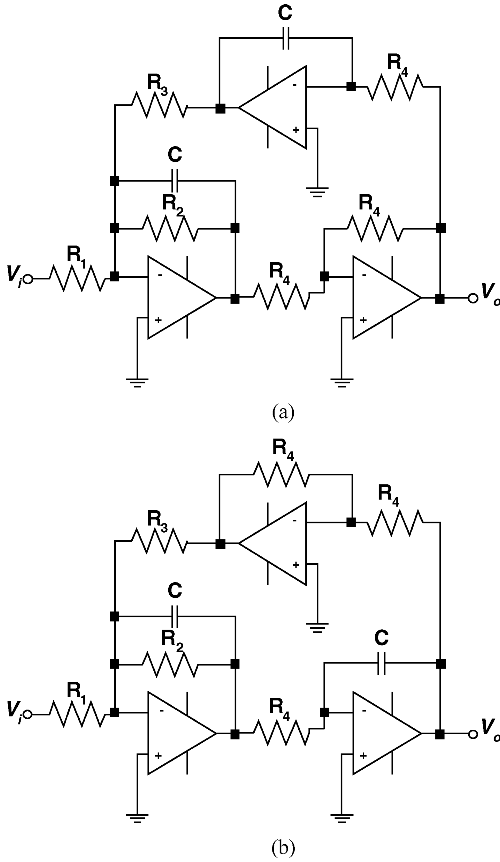

Fig. 4. Second-order biquad filters. (a) Biquad band-pass filter. (b) Biquad low-pass filter.

adopted in the demodulator circuit. Its transfer function can be represented as

$$\frac{V_o}{V_i} = \frac{A \cdot \omega_1^2}{s^2 + \frac{\omega_1}{Q}s + \omega_1^2} \tag{8}$$

where $A = R_3/R_1$, $\omega_1 = 1/R_3C$, and $Q = R_2/R_3$. The tunability and stability of these filters are particularly important when several stages are cascaded together.

The overall demodulator circuit is shown in Fig. 5. The primary input to this block is the output of the integrator, $\mathrm{V_{integ}}$. This is passed through two consecutive biquad band-pass filters. As the $2\omega_o$ frequency component of (6) is selected by the input stage of demodulation circuit, but only the ω_o reference is supplied, a frequency doubler must be built into the demodulator. This is implemented by using a squaring circuit, followed by a phase shifter and a band-pass filter. For the squaring circuit, a commercially available analog multiplier chip is used with both inputs shorted together. The processed input signal is multiplied by the output of this frequency doubler, and then low-pass filtered.

In the present manifestation of the circuit, $\mathrm{V_{dc}}$ is set at 5 V, and $\mathrm{V_{ac}}$ at 0.8 V. According to our previous investigations [14], the -3 dB frequency of thermal response of the probe is about 0.5 kHz with an open-loop interface circuit. It is somewhat higher with a closed loop interface circuit. The voltage dithering frequency, ω_o, is set at 1 kHz, in consideration for the thermal response time of the probe and the scan data bandwidth of 50 Hz (which has been experimentally verified, as discussed later). The Q factor of the band-pass filter and -3 dB frequency of the low-pass filter can be determined from these. (However, they need to be adjusted when low frequency noise exists near the band edge of the scan data.)

III. System Modeling and Simulation

To optimize the circuit, the entire system is modeled and simulated using the Simulink tool within MatLab (MatLab is a trademark of The MathWorks, Natick, MA USA). Its performance is estimated and the various circuit parameters are determined.

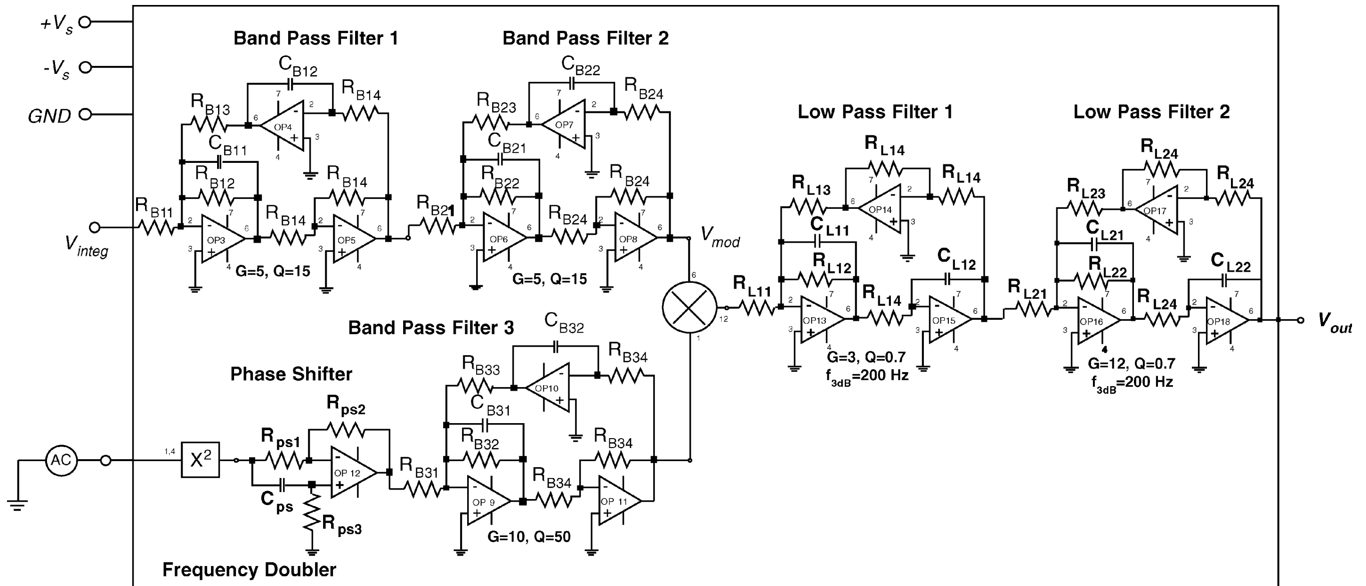

Fig. 5. Schematic of demodulator section of the interface circuit.

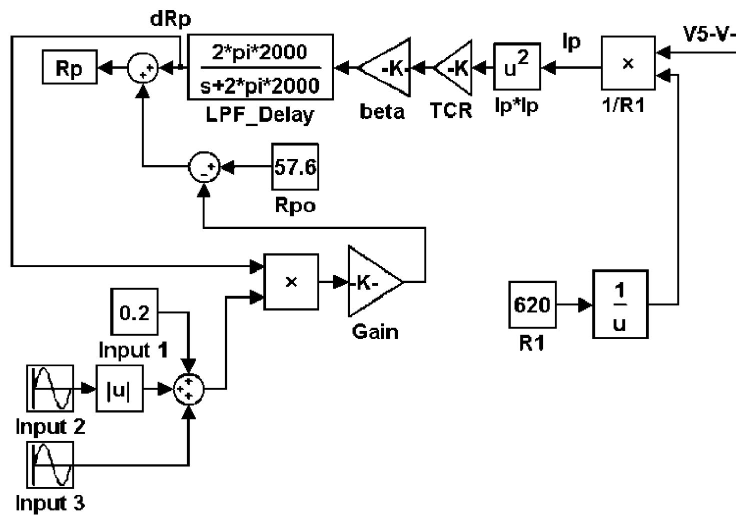

Fig. 6. Simulation model for a bolometer.

A Simulink model is needed for the probe to account for its interaction with the circuit, and it must be able to account not only for steady-state interactions, but also time varying ones for which it must account for the thermal delay. The thermal conductance, power, and temperature can be emulated by electrical conductance, current, and voltage, respectively. The consequent change in electrical voltage at a node is interpreted as a change in temperature at the corresponding location in the thermal system. Fig. 6 shows a one-dimensional (1-D) model, in which the probe temperature can be modulated by electrical power. Basically, the probe resistance is a sum of initial resistance R_{po} and resistance change dR_p due to the applied bias. Any further change in electrical resistance caused during a scan by a variation in the thermal conductance to the sample is compensated almost instantly by power from interface circuit and the probe temperature kept constant. The additional power needed for this is represented by the product of the normalized change in thermal conductance and the temperature bias ΔT between the probe and the sample. Since there is a finite delay between the supplied power and the resistance change due to the thermal capacitance of the probe shank and the sample specimen (even if the probe is in a constant temperature mode), a low-pass filter is used to imitate the thermal delay. The pole of this filter is adjusted to reflect experimental conditions, and can require some initial measurements to be made. The thermal time constant was obtained from a measurement in which the output signal amplitude was measured with respect to dithering frequency. There is a transition frequency of 1 kHz above which the signal amplitude starts dropping, and which can be used as bandwidth of the low pass filter in the model for the thermal probe and sample. As the dithering frequency is reduced, thermal delay can be ignored while SNR can be aggravated by $1/f$ noise. As the dithering frequency increases, thermal delay can cause signal distortion while $1/f$ noise can be suppressed.

It is also necessary to provide a model for the variation of thermal conductance encountered in a sample as the probe is

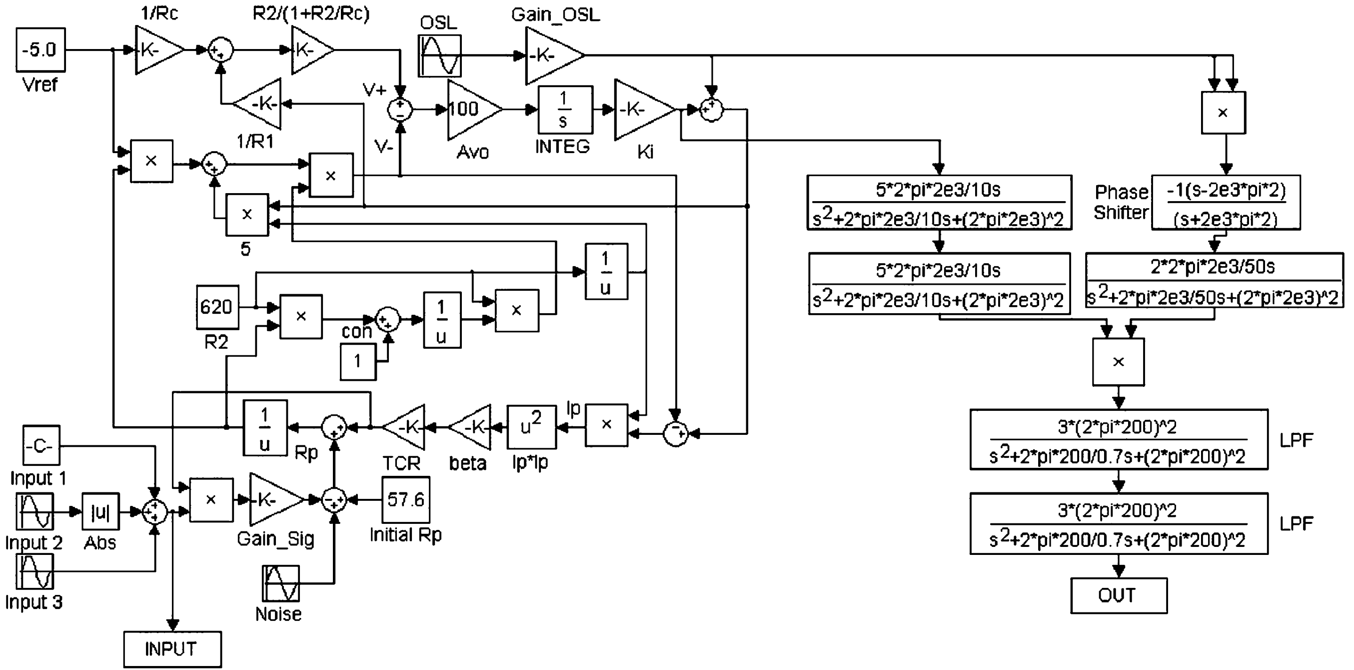

Fig. 7. State diagram for the scanning thermal microscopy sensing system.

scanned across it. The sum of a sinusoidal wave and its modulus, both with normalized sample conductance of 0.25 (unitless) in amplitude, and normalized dc sample conductance of 0.2 (unitless) has been empirically found to be suitable for emulating a sample with a periodic line-space photoresist pattern. To determine the impact that this change in thermal conductance of the sample has upon the electrical resistance of the bolometer, it is necessary first to multiply it by ΔT to obtain the change in heating power supplied by the probe, from that calculate the change in the average temperature of the bolometer by dividing by the absolute thermal conductance between the probe and the environment, and finally multiply this by the TCR. However, since all of these factors are embedded in dR_p, it is possible to simply multiply the normalized change in sample conductance by this quantity instead. The product appears in ohms, and can be directly subtracted from the total probe resistance.

The state diagram for the complete scanning thermal microscopy sensing system is presented in Fig. 7. The bolometer model is combined with models for the bridge circuit, PI controller, and the simple homodyne demodulator. One of the important optimization parameters to be simulated is the ratio of $I_{\rm dc}$ to $I_{\rm ac}$ in (3). As $I_{\rm ac}$ increases, modulation of probe resistance by the second harmonic of applied power cannot be ignored any more. In addition, the PI controller loses its feedback control in the simulation, even though the SNR at the output of demodulator improves in a certain range.

The simulated performance of the demodulator in terms of noise immunity is compared to the dc closed-loop interface circuit in Fig. 8. Fig. 8(a) shows the output of the dc closed loop interface circuit in the absence of a noise source, whereas Fig. 8(b) shows the output of ac closed loop interface circuit without the noise source. The two output signals are inverted, but are essentially similar when there is no low frequency noise. However, when 60 Hz noise with amplitude that is 20% of thermal input

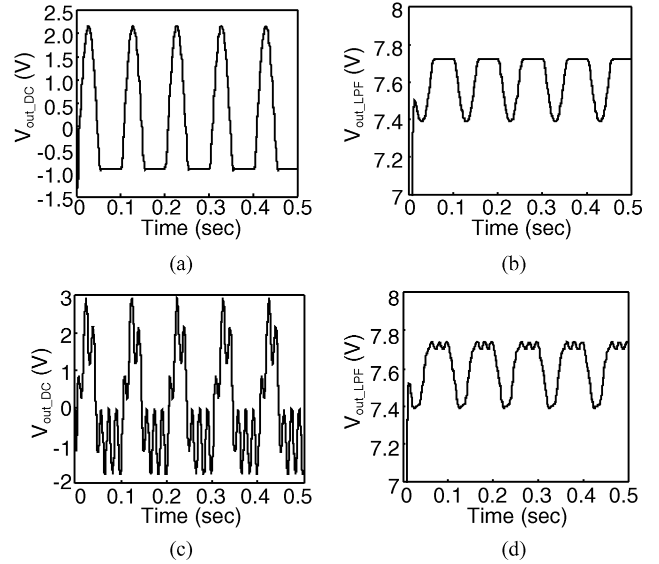

Fig. 8. Performance estimation for noise immunity in MatLab Simulink simulation. (a) Output signal of dc closed loop interface circuit without noise source. (b) Output signal of ac closed loop interface circuit without noise source. (c) Output signal of dc closed loop interface circuit with 60 Hz noise source corresponding to 10% of input signal. (d) Output signal of ac closed loop interface circuit with 60 Hz noise source corresponding to 10% of input signal.

signal is present, the output of dc closed loop circuit is corrupted significantly. In contrast, the electrical dithering used in the ac closed loop interface is relatively immune to the low frequency noise and provides a much better SNR.

The simulation of the whole sensing system provides better understanding of interaction between thermal reaction of the probe and electrical behavior of the interface circuit, and permits the evaluation of compromises in circuit configurations and operating parameters.

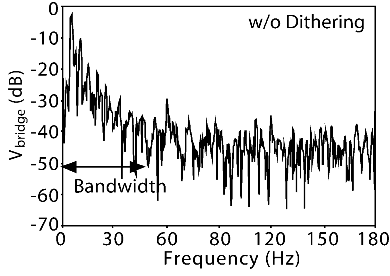

Fig. 9. Spectrum analysis during a real line scan across photoresist patterns.

IV. Experimental Measurement

Experimental measurements were carried out with the probe and interface circuit constructed as part of this research effort, but using a commercially available system (Topometrix SPMLab v.3.06) to provide the scanning and data acquisition. The test sample used in the evaluation of the circuit had a line-space pattern of 1 μm pitch and 218 nm thickness Shipley UV6 photoresist. As shown in Fig. 9, this sample produced a scanned data bandwidth of approximately 50 Hz. AC power was not supplied to the dithering system so that the probe temperature was kept constant during scanning. The scan speed was to 5–10 μm/s such that the bandwidth of the output signal, which is determined by topographical shape of sample, is narrow enough to avoid signal distortion during dithering and demodulation.

Frequency Spectrum Analysis: Fig. 10 shows the frequency spectra at various circuit nodes taken while scanning the test sample with a tip temperature of 45 °C. Fig. 10(a) shows that at the output of the bridge circuit, where the second harmonic contains the pursued power-modulated thermal signal, the amplitude ratio of the first harmonic to the second is 24.6, which is very close to the theoretical value of 25 obtained from (6). This demonstrates that the modulation frequency of 2 kHz is within the bandwidth of the system. Fig. 10(b) shows that the band-pass filtered signal has a dominant second harmonic. Filters with relatively high Q-factors of 10–15 were used to suppress other harmonics; a higher Q-factor could cause signal distortion due to reduced bandwidth. The total gain of each filter was set at 10–25. Fig. 10(c) shows the output of the frequency doubling circuit, which serves as the local oscillator in demodulation, and includes a squaring circuit, followed by a phase shifter and a band-pass filter. The phase shifter is used to adjust the phase of local oscillator to synchronize it to the input carrier. As noted previously, the phase mismatch between input carrier and local oscillator can cause signal distortion and reduction in signal amplitude. The dominant 2-kHz harmonic is obtained using a band-pass filter with a Q-factor of 50, which also removes the dc offset of the phase shifter. Fig. 10(d) shows the output of the multiplier, where both the downconverted and upconverted ($4\omega_o$) component contain information on conductance change across the sample. The former is pursued for the demodulated thermal signal. As shown in Fig. 10(e), the thermal signal is retrieved at the output of low-pass filters, and other harmonics are effectively removed. (The gain of the low-pass filter is restricted by its amplifiers and the dc offset of the mixer.)

Surface Scan: Fig. 11 shows the topographic and thermal images of the photoresist sample. The change in the compensation power delivered to the thermal probe is directly used to estimate the change of the thermal conductance of a sample. When the film is thin compared to the probe diameter, the heat transfer between the probe tip and silicon substrate can be modeled as that through a cylinder. Assuming that 1-D heat conduction from probe tip to sample, the heat loss (P_s) to the silicon substrate through the tip can be expressed as

$$P_s = \frac{(T_{\rm tip} - T_0) \cdot A_0 \cdot k_s}{H} \tag{9}$$

where $T_{\rm tip}$ is the probe tip temperature, A_0 is the tip-sample contact area, k_s is the thermal conductivity of photoresist, and H is the photoresist thickness. In cases for which the thickness of the conductive layer exceeds the tip diameter, a $\text{correction factor} > 1$ must be incorporated into the numerator. Thermal conductance is defined as $A_0 \cdot k_s/H$. This formula assumes that the substrate of the sample, i.e., the material below the thin film, remains at T_0, the room temperature. The compensation power P_c delivered to the thermal probe and sample to keep the probe average temperature at T_p is given by

$$P_c = \left(\frac{V_{\rm bridge} - V_{\rm ref}}{R_1 + R_p}\right)^2 \cdot R_p. \tag{10}$$

Therefore, the change in thermal conductance of sample during a scan can be represented as

$$\Delta G = \frac{P_{c1} - P_{c2}}{T_{\rm tip} - T_o} = \left[\left(\frac{V_{\rm bridge1} - V_{\rm ref}}{R_1 + R_p}\right)^2 - \left(\frac{V_{\rm bridge2} - V_{\rm ref}}{R_1 + R_p}\right)^2\right] \cdot \frac{R_p}{T_{\rm tip} - T_o} \quad \left(\frac{W}{K}\right). \tag{11}$$

This formula can be used to calculate the variation of thermal conductance across a sample by measuring the variation in power dissipated for a constant temperature map. Even though P_s is not equal to P_c, ΔP_s is regarded as equal or very close to ΔP_c because the wasted heat loss through probe shank can be considered constant in constant temperature operation. Thus, mapping the power in constant temperature mode provides an accurate representation of the change in thermal conductance of the sample.

The full scale thermal conductance change can be calculated from (11). For the thermal image of Fig. 11(b), R_1 and R_p are 250 Ω and 25 Ω. The reference voltage $V_{\rm ref}$ is -4.0 V and T_p is 318 K. The voltage at the top of the bridge, $V_{\rm bridge}$, is equal to the output voltage divided by the voltage gain of 100. The calculated variation in thermal conductance from Si substrate through the photoresist film is 1.5×10^{-7} W/K. This calculation assumes that the thermal conductivity of UV6 is 0.193 W/mK [8], and is close to that of polymethyl methacrylate (PMMA). The topographic and thermal images appear similar because the thermal conductance change is predominantly due to the topographical change of sample. Fig. 12 shows the variations in

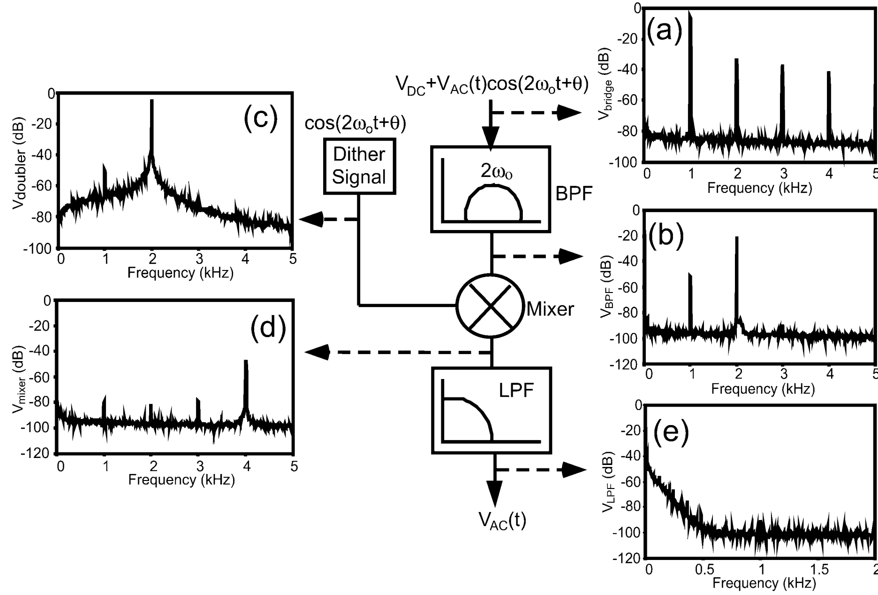

Fig. 10. Frequency response at various nodes of the demodulator.

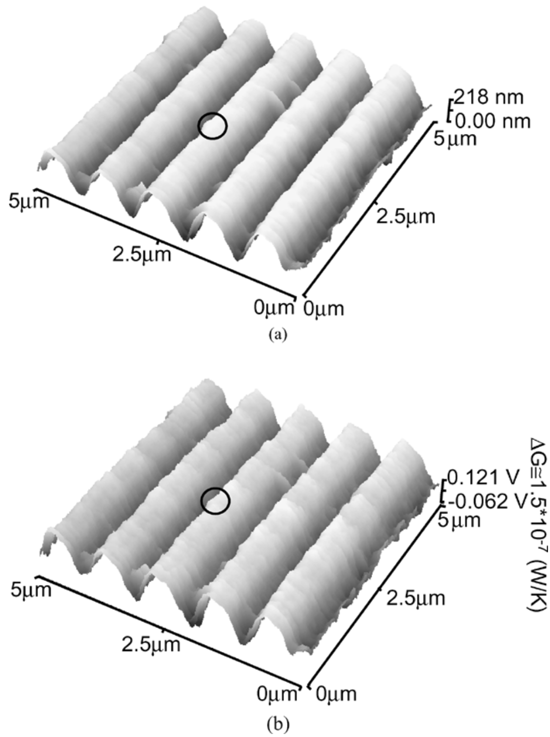

Fig. 11. (a) Topographic and (b) thermal images of developed Shipley UV6 photoresist sample with 218 nm in thickness scanned at 45 °C tip temperature.

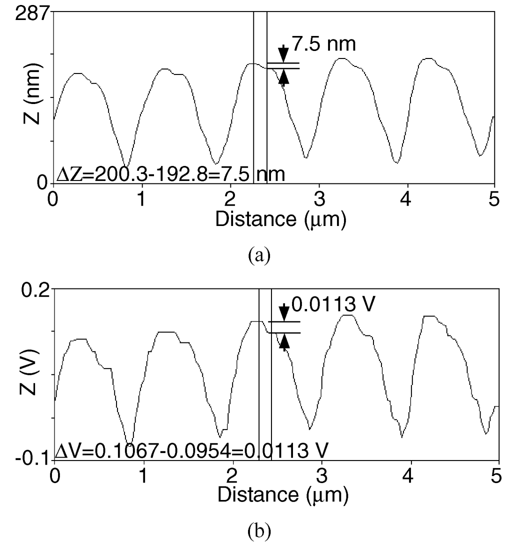

Fig. 12. Scan results of developed 218-nm-thick Shipley UV6 photoresist scanned at 45°C tip temperature using ac dithering interface circuit. (a) Topographic line scan across photoresist patterns. (b) Thermal line scan across photoresist patterns.

topographic and thermal signal across photoresist line patterns. The SNR is 15.7 for the thermal measurement. The resolved thermal conductance change is calculated as 2.9×10^{-11} W/K for a thickness change of 7.5 nm based on (9). The noise-equivalent change in thermal conductance (at which the SNR drops to unity), is < 3 pW/K. The specifications of the thermal sensing system are summarized in Table I and performance of micromachined bolometer is summarized in Table II. Throughout the

TABLE I
SPECIFICATIONS OF THE THERMAL SENSING SYSTEM

Resistance-Dithering Frequency	1 kHz
Voltage-Modulation Frequency	2 kHz
Maximum V_{CC} (V_{EE})	±18 V
Minimum V_{CC} (V_{EE})	±5.0 V
V_{ref}	-4.0 V
Signal Bandwidth	≈50 Hz
Maximum Probe Current (I_{max})	35 mA
Operating Probe Current (I_p)	10 mA
Maximum Probe Tip Temperature (T_{max})	160 °C
Operating Probe Tip Temperature (T_p)	≈45 °C

TABLE II
SUMMARY OF MEASURED PERFORMANCE FOR A MICROMACHINED POLYIMIDE BOLOMETER, AS TESTED ON PHOTORESIST SAMPLES

Performance	AC Closed-Loop Circuit
Tip Diameter	≈50 nm
Lateral Spatial Resolution	<50 nm [Li03]
Topographical Resolution	≈1 nm [Li03]
SNR for UV6 218 nm thickness	15.7
ΔR Resolution	<0.56 mΩ (controllable)
Tip Temperature Resolution	<2.5 mK (controllable)
Detectable Thermal Conductance Change	<3 (pW/K)

experiment, the scan rate was kept at 10 $\mu m/s$ and the bandwidth of about 50 Hz was measured for the detectable thermal conductance change.

In contrast with the micromachined polyimide probe, for a Wollaston wire probe the nominal resistance and spring constant are 2.1 Ω and 5 N/m, respectively. Since the diameter of this probe is 100 × larger than that of the micromachined probe, its minimum detectable thermal conductance is estimated to be about 10^4 times larger because the detectable thermal conductance change is linearly proportional to tip area when the detectable limit of topographic change is the same.

V. CONCLUSION

This effort has demonstrated that low-frequency electrical dithering of the tip temperature can be used with ultracompliant polyimide probes, and that an interface circuit which uses a PI controller for temperature stabilization and homodyne demodulation of the second harmonic dither component is effective and relatively immune to noise. The temperature controllability provided by the sensing interface circuit extends the applications of the thermal probes to thermal analysis of material properties. The electrical model for the thermal probe combined with that of interface circuit provides understanding on thermal and electrical interaction between probe and interface circuit and permits design choices and operating conditions to be evaluated. Frequency spectrum analysis at critical nodes of the circuit obtained during operation of the system confirms that modulation and demodulation of thermal signal are successfully achieved by the circuit and probe. Scanning thermal images obtained show a SNR of 15.7 for 218 nm thick UV photoresist; the thermal conductance change is 29 pW/K, and the noise limit is $< 3 \text{ pW/K}$.

ACKNOWLEDGMENT

Valuable discussions with Dr. M.-H. Li are gratefully acknowledged. The authors are also grateful to Prof. F. Cerrina for helping to motivate this effort, and for supplying the UV6 photoresist samples.

REFERENCES

[1] J. R. Barnes, R. J. Stephenson, C. N. Woodburn, S. J. O'Shea, M. E. Welland, T. Rayment, J. K. Gmzewski, and C. Gerber, "A femtojoule calorimeter using micromechanical sensors," *Rev. Sci. Instrum.*, vol. 65, no. 12, pp. 3793–3798, 1994.
[2] R. C. Davis, C. C. Williams, and P. Neuzil, "Micromachined submicrometer photodiode for scanning probe microscopy," *Appl. Phys. Lett.*, vol. 66, no. 18, pp. 2309–2311, 1995.
[3] R. B. Dinwiddie, R. J. Pylkki, and P. E. West, "Thermal conductivity contrast imaging with a scanning thermal microscope," *Thermal Conductivity*, vol. 22, pp. 668–677, 1994.
[4] G. B. M. Fiege, A. Altes, R. Heiderhoff, and L. J. Balk, "Quantitative thermal conductivity measurements with nanometer resolution," *J. Phys. D: Appl. Phys.*, vol. 32, pp. L13–L17, 1999.
[5] D. Fryer, P. Nealey, and J. de Pablo, "Thermal probe measurements of the glass transition temperature for ultrathin polymer films as a function of thickness," *Macromolecules*, vol. 33, no. 17, pp. 6439–47, 2000.
[6] ——, "Scaling of T_g and reaction rate with film thickness in photoresist: A thermal probe study," *J. Vac. Sci. Technol. B*, vol. 18, no. 6, pp. 3376–3380, 2000.
[7] Y. B. Gianchandani and K. Najafi, "A silicon micromachined scanning thermal profiler with integrated elements for sensing and actuation," *IEEE Trans. Electron Devices*, vol. 44, pp. 1857–1867, 1997.
[8] A. Hammiche, D. J. Hourston, H. M. Pollock, M. Reading, and M. Song, "Scanning thermal microscopy: Subsurface imaging, thermal mapping of polymer blends, and localized calorimetry," *J. Vac. Sci. Technol. B*, vol. 14, no. 2, pp. 1486–1491, 1996.
[9] A. Hammiche, H. M. Pollock, M. Song, and D. J. Hourston, "Sub-surface imaging by scanning thermal microscopy," *Meas. Sci. Technol.*, vol. 7, pp. 142–150, 1996.
[10] J.-H. Lee, "A Microbolometer-Based Scanning Thermal Microscopy System with Servo-Controlled Interface Circuitry," Ph.D., University of Wisconsin, 2003.
[11] J.-H. Lee and Y. B. Gianchandani, "A scanning thermal microscopy system with a temperature dithering, servo-controlled interface circuit," in *IEEE Int. Symp. Circuits Syst.*, May 2003, pp. IV812–IV815.
[12] T. Leinhos, M. Stopka, and E. Oesterschulze, "Micromachined fabrication of Si cantilevers with Schottky diodes integrated in the tip," *Appl. Phys. A*, vol. 66, pp. S65–S69, 1998.
[13] M.-H Li and Y. B. Gianchandani, "Microcalorimetry applications of a surface micromachined bolometer-type thermal probe," *J. Vac. Sci. Technol. B*, vol. 18, no. 6, pp. 3600–3603, 2000.
[14] M.-H. Li, J. J. Wu, and Y. B. Gianchandani, "Surface micromachined polyimide scanning thermocouple probes," *J. Microelectromech. Syst.*, vol. 10, no. 1, pp. 3–9, 2001.
[15] M.-H Li and Y. B. Gianchandani, "Applications of a low contact force polyimide shank bolometer probe for chemical and biological diagnostics," *Sens. Actuators, A (Physical)*, vol. 104, pp. 236–245, Apr. 2003.
[16] L. Lu, W. Yi, and D. L. Zhang, "3ω method for specific heat and thermal conductive measurements," *Rev. Sci. Instrum.*, vol. 72, no. 7, pp. 2996–3003, 2001.
[17] K. Luo, Z. Shi, J. Varesi, and A. Majumdar, "Sensor nanofabrication, performance, and conduction mechanisms in scanning thermal microscopy," *J. Vac. Sci. Technol. B*, vol. 15, no. 2, pp. 349–360, 1997.
[18] A. Majumdar, J. Lai, M. Chandrachood, O. Nakabeppu, Y. Wu, and Z. Shi, "Thermal imaging by atomic force microscopy using thermocouple cantilever probes," *Rev. Sci. Instrum.*, vol. 66, no. 6, pp. 3584–3592, 1995.
[19] A. Majumdar, "Scanning thermal microscopy," *Annu. Rev. Mater. Sci.*, vol. 29, pp. 505–585, 1999.
[20] G. Mills, H. Zhou, A. Midha, L. Donaldson, and J. M. R. Weaver, "Scanning thermal microscopy using batch fabricated thermocouple probes," *Appl. Phys. Lett.*, vol. 72, no. 22, pp. 2900–2902, 1998.
[21] I. K. Moon, Y. H. Jeong, and S. I. Kwun, "The 3ω technique for measuring dynamic specific heat and thermal conductivity of a liquid or solid," *Rev. Sci. Instrum.*, vol. 67, no. 1, pp. 29–35, 1996.
[22] O. Nakabeppu, M. Chandrachood, Y. Wu, J. Lai, and A. Majumdar, "Scanning thermal imaging microscopy using composite cantilever probes," *Appl. Phys. Lett.*, vol. 66, no. 6, pp. 694–696, 1995.
[23] L. E. Ocola, D. Fryer, P. Nealey, J. dePablo, F. Cerrina, and S. Kämmer, "Latent image formation: Nanoscale topography and calorimetric measurements in chemically amplified resists," *J. Vac. Sci. Technol. B*, vol. 14, no. 6, pp. 3974–3979, 1996.
[24] E. Oesterschulze and M. Stopka, "Imaging of thermal properties and topography by combined scanning thermal and scanning tunneling microscopy," *Microelectron. Eng.*, vol. 31, pp. 241–248, 1996.
[25] A. J. Peyton and V. Walsh, *Analog Electronics with OP Amps*, Cambridge, 1993, pp. 18–24.
[26] L. Shi, O. Kwon, G. Wu, and A. Majumdar, "Quantitative thermal probing of devices at sub-100 nm resolution," in *IEEE Ann. Int. Reliability Phys. Symp.*, 2000, pp. 394–398.
[27] Y. Suzuki, "Novel microcantilever for scanning thermal imaging microscopy," *Japan. J. Appl. Phys.*, pt. 2, vol. 35, no. 3A, pp. L352–L354, 1996.

[28] Veeco.. [Online]. Available: www.veeco.com
[29] P. Vettiger *et al.*, "The "Millipede"—More than one thousand tips for future AFM data storage," *IBM J. Res. Develop.*, vol. 44, no. 3, pp. 323–340, 2000.
[30] H. K. Wickramasinghe, "Scanned-probe microscopes," *Scientif. Amer.*, pp. 98–105, Oct. 1989.
[31] H. Zhou, A. Midha, G. Mills, S. Thoms, S. K. Murad, and J. M. R. Weaver, "Generic scanned-probe microscope sensors by combined micromachining and electron-beam lithography," *J. Vac. Sci. Technol. B*, vol. 16, no. 1, pp. 54–58, 1998.

Joohyung Lee received the B.S. and M.S. degrees in electrical and computer engineering from Pohang Institute of Science and Technology (POSTECH), Korea, in 1991 and 1993, respectively, and the Ph.D. degree in electrical and computer engineering from the University of Wisconsin, Madison, in 2003.

He is currently with Samsung Electronics Co., Ltd., Gyeonggi-Do, Korea, as a senior engineer working in the area of optical and physical sensor array.

Yogesh B. Gianchandani (S'83–M'85–SM'04) received the B.S., M.S, and Ph.D. degrees in electrical engineering, with a focus on microelectronics and MEMS.

He is presently an Associate Professor with the EECS Department, University of Michigan, Ann Arbor, and also holds a joint appointment with the Mechanical Engineering Department. He also serves as the director of the College of Engineering Interdisciplinary Professional Degree Program in Integrated Microsystems. Prior to this, he was with the ECE Department, University of Wisconsin, Madison. He has also held industry positions with Xerox Corporation, Microchip Technology, and other companies, working in the area of integrated circuit design. His research interests include all aspects of design, fabrication, and packaging of micromachined sensors and actuators and their interface circuits.

Prof. Gianchandani serves on the editorial boards of *Sensors and Actuators, IOP Journal of Micromechanics and Microengineering,* and the *Journal of Semiconductor Technology and Science*. He also served on the steering and technical program committees for the IEEE/ASME International Conference on Micro Electro Mechanical Systems (MEMS) for some years, and served as a General Co-Chair for this meeting in 2002.